



COMMUNICATIONS PHYSICS

ARTICLE

<https://doi.org/10.1038/s42005-019-0218-5>

OPEN

Quantum spacetime on a quantum simulator

Keren Li^{1,2,3,4,15}, Youning Li^{3,4,15}, Muxin Han^{5,6,15}, Sirui Lu^{1,4}, Jie Zhou^{7,8}, Dong Ruan⁴, Guilu Long^{4,9,10}, Yidun Wan^{1,2,11,12,13*}, Dawei Lu^{1,2*}, Bei Zeng^{1,2,3,14*} & Raymond Laflamme^{3,7}

Quantum simulation has shown its irreplaceable role in many fields, where it is difficult for classical computers to do much. On a four-qubit Nuclear Magnetic Resonance (NMR) quantum simulator, we experimentally simulate the spin-network states by simulating quantum spacetime tetrahedra. The fidelities of our experimentally prepared quantum tetrahedra are all above 95%. We then use the quantum tetrahedra prepared by the Nuclear Magnetic Resonance to simulate a spinfoam vertex amplitude, which displays the local dynamics of quantum spacetime. By measuring the geometric properties on the corresponding quantum tetrahedra and simulating their interaction, our experiment serves as a basic module that represents the Feynman diagram vertex in the spinfoam formulation of Loop Quantum Gravity(LQG). This is an initial attempt to study LQG by quantum information processing.

¹Center for Quantum Computing, Peng Cheng Laboratory, Shenzhen 518055, China. ²Shenzhen Institute for Quantum Science and Engineering, and Department of Physics, Southern University of Science and Technology, Shenzhen 518055, China. ³Institute for Quantum Computing and Department of Physics and Astronomy, University of Waterloo, Waterloo, ON, Canada N2L 3G1. ⁴State Key Laboratory of Low-Dimensional Quantum Physics and Department of Physics, Tsinghua University, Beijing 100084, China. ⁵Department of Physics, Florida Atlantic University, 777 Glades Road, Boca Raton, FL 33431, USA. ⁶Institut für Quantengravitation, Universität Erlangen-Nürnberg, Staudtstr. 7/B2, 91058 Erlangen, Germany. ⁷Perimeter Institute for Theoretical Physics, Waterloo, ON, Canada N2L 2Y5. ⁸YMSC, Tsinghua University, Beijing 100084, China. ⁹Beijing Academy of quantum information science, Beijing 100193, China. ¹⁰Beijing National Research Center of Information Science and Technology, Beijing 100084, China. ¹¹State Key Laboratory of Surface Physics, Fudan University, Shanghai 200433, China. ¹²Department of Physics and Center for Field Theory and Particle Physics, Fudan University, Shanghai 200433, China. ¹³Institute for Nanoelectronic devices and Quantum computing, Fudan University, Shanghai 200433, China. ¹⁴Department of Mathematics and Statistics, University of Guelph, Guelph, ON, Canada N1G 2W1. ¹⁵These authors contributed equally: Keren Li, Youning Li, Muxin Han. *email: ydwan@fudan.edu.cn; ludw@sustech.edu.cn; zengb@uoguelph.ca.

As the quantum system size grows linearly, the corresponding Hilbert space grows exponentially. Therefore, it is impossible for classical computers to study large quantum systems, although they have gained plenty of success in the simulation of a variety of physical systems. A raising hope to overcome the issue is by using quantum computers. Since quantum computers process information intrinsically or quantum-mechanically, they are expected to outperform their classical counterparts exponentially. As first defined by Feynman in 1982¹, quantum computers are certain quantum systems that can be easily controlled to imitate the behaviors or properties of other less accessible quantum systems^{2,3}. Here, we demonstrate how nuclear magnetic resonance (NMR), with a high controllable performance on the quantum system⁴, can be used to develop simulation methods^{5,6} for exhibiting quantum geometries of space and spacetime, based on the analogies between nuclei spin states in NMR samples and spin-network states in quantum gravity.

Quantum gravity aims at unifying the Einstein gravity with quantum mechanics, such that our understanding of gravity can be extended to the Planck scale 1.22×10^{19} GeV^{7,8}. At the Planck level, Einstein gravity and the continuum of spacetime break down and are replaced by a quantum spacetime. Many current approaches toward quantum spacetimes are rooted in spin networks—an important, non-perturbative framework of quantum gravity. Spin networks were proposed by Penrose, as motivated by the twistor theory⁹, and later have been widely applied to loop quantum gravity (LQG)¹⁰. In LQG, spin networks are quantum states representing fundamentally discrete quantum geometries of space at the Planck scale¹¹, serving as the boundary data of certain 3 + 1 dimensional quantum spacetime. A spin network is represented by a graph, whose (oriented) links and nodes are colored by spin halves. Any node with edges corresponds to a geometry. For example, a graph consists of a number of four-valent (or generally n-valent) nodes, each of which corresponds to a quantum tetrahedron geometry¹².

A 3 + 1 dimensional quantum spacetime whose boundary is a spin network is a spinfoam, a “network” consisting of a number of three-dimensional world sheets (surfaces) and their intersections, where the world sheets are colored by spin halves. Just like the time evolution of a classical space that builds up a classical spacetime, the time evolution of a spin network forms a quantum spacetime^{13,14}. Examples of quantum spacetimes are shown in Fig. 1a, b. Each vertex where the world sheets meet leads to a quantum transition that changes the spin network and represents local dynamics (interactions) of quantum geometry. Similar to Feynman diagrams, quantum spacetimes encode the transition amplitudes—spinfoam amplitudes—between the initial and final spin networks^{15–17}. A spinfoam amplitude of a quantum spacetime is determined by the vertex amplitudes locally encoded in the intersection vertices in the quantum spacetime (Fig. 1c, d). Thus, quantum spacetimes and spinfoam amplitudes provide a consistent and promising approach to quantum gravity.

In this paper, by using 4-qubit quantum registers in the NMR system, $SU(2)$ invariant-tensor states representing the quantum tetrahedra are created with over 95% fidelity, and we subsequently measure their geometrical properties—dihedral angles, which determine the shapes of tetrahedra. This simulation with NMR is featured by the capability of controlling individual qubits with high precision. With these quantum tetrahedra, we simulate a spin-1/2 spinfoam vertex amplitude in Ooguri’s model. Quantum tetrahedra and vertex amplitudes serve as building blocks of LQG. Our work opens up a new window of putting LQG in experiments.

Results

Quantum tetrahedron. Given a spin network defined on an oriented graph Γ , each link l is oriented and carries a half-integer j_l , which labels a $2j_l + 1$ dimensional $SU(2)$ irreducible representation space \mathcal{H}_{j_l} . Each node n carries a tensor $|i_n\rangle$ in the tensor representation $\otimes_l \mathcal{H}_{j_l}$, that is invariant under $SU(2)$ action. The state $|i_n\rangle$ is thus referred to as an invariant tensor. A spin-network state is written as a triple $|\Gamma, j_l, i_n\rangle$, defined by a tensor product of the invariant tensors $|i_n\rangle$ at all nodes, $|\Gamma, j_l, i_n\rangle := \otimes_n |i_n\rangle$, where spin labels of $|i_n\rangle$ are implicit. All spin networks with arbitrary Γ, j_l, i_n define an orthonormal basis in the Hilbert space of LQG. Thus, simulating a spin network with m nodes, $\otimes_{n=1}^m |i_n\rangle$, only amounts to producing m invariant tensors $|i_1\rangle, \dots, |i_m\rangle$ in the experiment. It then suffices to simulate $|i_n\rangle$.

The rank N of $|i_n\rangle$ coincides with the valence of the node n . The $SU(2)$ invariance of a rank- $N|i_n\rangle$ implies

$$(\hat{\mathbf{J}}^{(1)} + \hat{\mathbf{J}}^{(2)} + \hat{\mathbf{J}}^{(3)} + \dots + \hat{\mathbf{J}}^{(N)})|i_n\rangle = 0. \quad (1)$$

Here, $\hat{\mathbf{J}}^{(k)} = (\hat{J}_x^{(k)}, \hat{J}_y^{(k)}, \hat{J}_z^{(k)})$ are the angular momentum operators on the Hilbert space \mathcal{H}_{j_k} . These operators satisfy $[\hat{J}_a^{(m)}, \hat{J}_b^{(k)}] = i\delta^{mk}\epsilon_{abc}\hat{J}_c^{(k)}$, where ϵ_{abc} is the Levi-Civita symbol. Eq. (1) is the internal gauge invariance of LQG, as the remnant from restricting the local Lorentz symmetry in a spatial slice^{10,18}. As Euclidean tetrahedra with $N = 4$ are the fundamental building blocks of arbitrary curved 3d discrete geometries, in this paper, we mainly focus on $N = 4$. In a 3d Euclidean space, a tetrahedron gives 4 oriented areas $\mathbf{E}^{(k=1,\dots,4)} = (E_x^{(k)}, E_y^{(k)}, E_z^{(k)})$, where $|\mathbf{E}^{(k)}|$ is the area of the k th face, and $\mathbf{E}^{(k)}/|\mathbf{E}^{(k)}|$ is the unit vector normal to the face. Four tetrahedron faces form a closed surface, namely

$$\mathbf{E}^{(1)} + \mathbf{E}^{(2)} + \mathbf{E}^{(3)} + \mathbf{E}^{(4)} = 0. \quad (2)$$

Conversely, the data $\mathbf{E}^{(k=1,\dots,4)}$ subject to Eq. (2) uniquely determine the (Euclidean) tetrahedron geometry¹⁹. The comparison of Eqs. (1) and (2) indicates that $\hat{\mathbf{J}}^{(k)}$ is the quantum version of $\hat{\mathbf{E}}^{(k)}$. In fact in LQG, area operators \mathbf{E}^k are related to $\hat{\mathbf{J}}^{(k)}$ by $\hat{\mathbf{E}}^{(k)} = 8\pi\ell_p^2 \hat{\mathbf{J}}^{(k)}$, where $\ell_p = G_N \hbar$ is the Planck length, and G_N the Newton’s constant. Hence, Eqs. (1) and (2) lead to a geometrical interpretation for the invariant tensor, and further for the spin network²⁰. More detailed physical account for this quantization is given in Supplementary Note 1.

Quantum spacetime atom. In a 3 + 1 dimensional dynamical quantum spacetime shown in Fig. 1b, we consider an atom of quantum spacetimes, namely a 3-sphere enclosing a portion of the quantum spacetime surrounding a vertex. The boundary of the enclosed quantum spacetime is precisely a spin network (see Fig. 1c). Large quantum spacetimes with many vertices can be obtained by gluing the atoms.

A vertex amplitude associated with a quantum spacetime atom, which determines the spinfoam amplitude, is an evaluation of the spin network $\otimes_{n=1}^5 |i_n\rangle$, leading to a transition from the initial to the final spin networks. The evaluation itself is a function of invariant tensors. The spin network $\otimes_{n=1}^5 |i_n\rangle$ in Fig. 1c shows the (quantum) gluing of 5 tetrahedra to form a closed S^3 , where each invariant tensor associates with a node in the spin network (blue in Fig. 1c). Consider the following evaluation of $\otimes_{n=1}^5 |i_n\rangle$ by picking up the 2-qubit maximally entangled state $|\epsilon_l\rangle = (|01\rangle - |10\rangle)/\sqrt{2}$

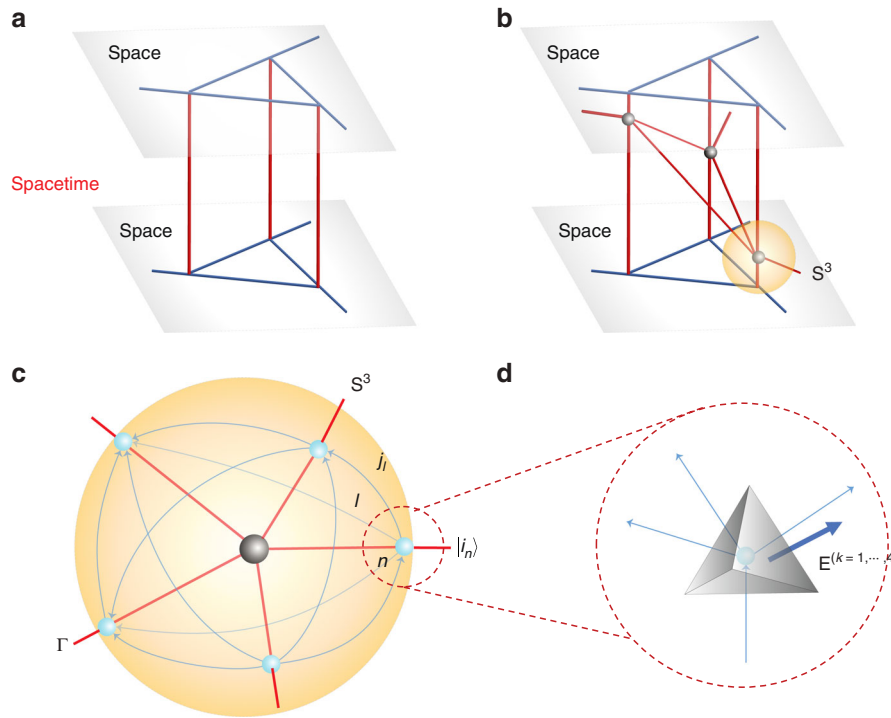


Fig. 1 Quantum spacetime and tetrahedra. **a** A static 4d quantum spacetime from evolving the spin network. **b** A dynamical quantum spacetime with a number of five valent vertices (in black) by intersecting world sheets, one of which is denoted by S^3 . **c** The local structure of a vertex from **b** by considering a 3-sphere S^3 enclosing the vertex. Intersections between the world sheets and S^3 give a spin network (in blue). Each spin network represents a state $|i_n\rangle$ and each link l is oriented, which carries a half-integer j_l . **d** Quantum geometrical tetrahedra. Each node of the spin network represents a quantum tetrahedron. Connecting 2 nodes by a link in the spin network corresponds to gluing 2 tetrahedra through the face dual to the link. Oriented areas are denoted $\mathbf{E}^{(k=1,\dots,4)} = (E_x^{(k)}, E_y^{(k)}, E_z^{(k)})$ here

for each link l

$$A(i_1, \dots, i_5) = \bigotimes_{l=1}^{10} \left\langle \epsilon_l \left| \bigotimes_{n=1}^5 i_n \right. \right\rangle. \quad (3)$$

The inner product above takes place at the end points of each l , between a qubit in $|\epsilon_l\rangle$ and the other in $|i_n\rangle$. Each link in the spin network corresponds to gluing a pair of faces belonging to two different quantum tetrahedra. Gluing faces requires to match in their quantum area, but does not require to match in shape due to quantum fluctuations.

The resulting $A(i_1, \dots, i_5)$ is a vertex amplitude of quantum spacetime in Ooguri's model¹⁵, where the spins are all $1/2$. Ooguri's model defines a topological invariant of four-manifolds, and the vertex amplitudes in Ooguri's model relate to the classical action of gravity when (1) the spins are large and (2) spins and invariant tensors $|i_n\rangle$ satisfy Regge-like boundary conditions²¹. $A(i_1, \dots, i_5)$ is the transition amplitude from m to $5-m$ quantum tetrahedra ($m < 5$), or covariantly, the interaction amplitude of 5 quantum tetrahedra. The amplitude describes the local dynamics of LQG in the $3+1$ dimensional quantum spacetime enclosed by the S^3 .

Experimental design. LQG identifies quantum tetrahedron geometries with the quantum angular momenta subject to Eq. (1). This identification enables us to simulate quantum geometries with quantum registers. We focus on the situation with all spins $j = 1/2$ ($\mathcal{H}_{j=1/2} \simeq \mathbb{C}^2$) and simulate quantum tetrahedra ($N = 4$) with four-qubit invariant-tensor states (details are given in Supplementary Note 2).

The quantum tetrahedra can be reconstructed through various geometrical properties defined by the operators on

$\text{Inv}_{\text{SU}(2)}[\mathcal{H}_{j=1/2}^{\otimes 4}]$. For example, with the quantization of area operators $\hat{\mathbf{E}}^{(k)}$, the quantum area of the k th face is diagonalized^{11,22} as

$$\widehat{\mathbf{A}\mathbf{r}}_k \equiv \sqrt{\hat{\mathbf{E}}^{(k)} \cdot \hat{\mathbf{E}}^{(k)}} = 8\pi\ell_P^2 \sqrt{\hat{\mathbf{J}}^{(k)} \cdot \hat{\mathbf{J}}^{(k)}}. \quad (4)$$

The expectation value of an area operator in an invariant tensor $|i\rangle$ is $\langle i | \widehat{\mathbf{A}\mathbf{r}}_k | i \rangle = 8\pi\ell_P^2 \sqrt{3/4}$. In addition, the angle θ_{km} between the k th and m th face normals is quantized accordingly²³ as

$$\widehat{\cos \theta_{km}} = \frac{\hat{\mathbf{E}}^{(k)} \cdot \hat{\mathbf{E}}^{(m)}}{\sqrt{\hat{\mathbf{E}}^{(k)} \cdot \hat{\mathbf{E}}^{(k)}} \sqrt{\hat{\mathbf{E}}^{(m)} \cdot \hat{\mathbf{E}}^{(m)}}} = \frac{4}{3} \hat{\mathbf{J}}^{(k)} \cdot \hat{\mathbf{J}}^{(m)}. \quad (5)$$

The dihedral angle ϕ_{km} between the k th and m th faces relates to θ_{km} by $\cos \phi_{km} = -\cos \theta_{km}$. Because of Eq. (1), for a certain k , there are only two independent expectation values of $\widehat{\cos \theta_{km}}$, say, $\langle i | \widehat{\cos \theta_{12}} | i \rangle$ and $\langle i | \widehat{\cos \theta_{13}} | i \rangle$. For the arbitrary tetrahedron $|i\rangle$, its geometry can be uniquely determined by the expectation values of the four areas and two dihedral angles (Supplementary Note 3).

Since $\text{Inv}_{\text{SU}(2)}[\mathcal{H}_{j=1/2}^{\otimes 4}]$ is two-dimensional, this invariant-tensor space can be presented on a Bloch sphere. With the spherical coordinate system, any point (θ, ϕ) on the surface can uniquely determine a quantum tetrahedron. In our experiments, we intend to simulate ten quantum tetrahedra by preparing the corresponding invariant-tensor states. These states are labeled by 10 colored points on the Bloch sphere, as shown in Fig. 2, whose spherical coordinates can be found in Supplementary Note 4.

Our experiments were conducted on a 700-MHz DRX Bruker spectrometer at room temperature. The crotonic acid molecule with four ^{13}C nuclei, works as our four-qubit quantum system,

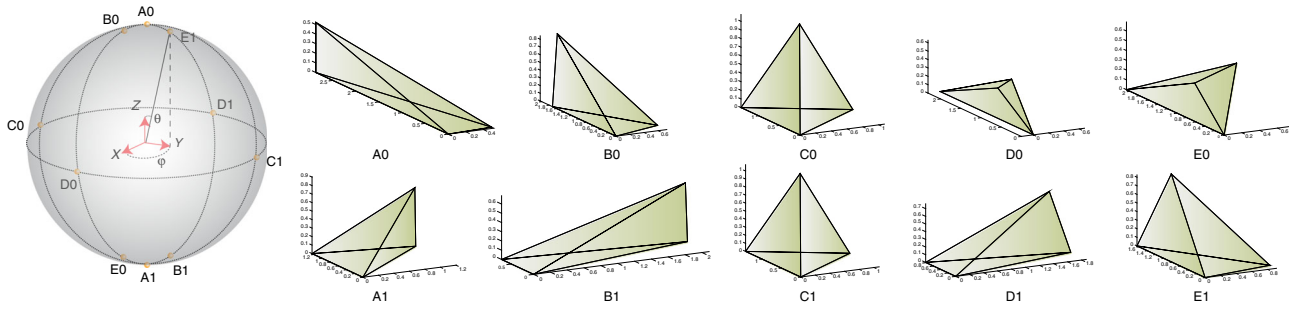


Fig. 2 Experimentally prepared states on the Bloch sphere and their corresponding classical tetrahedra. The states take the form $\cos \frac{\theta}{2} |0\rangle_L + e^{i\phi} \sin \frac{\theta}{2} |1\rangle_L$ and are labeled by $A_i, B_i, C_i, D_i, E_i (i = 0, 1)$, among which, C_0 and C_1 are regular tetrahedrons. $|0_L\rangle$ and $|1_L\rangle$ are the basis states in a subspace of a four-qubit system, representing a single logical qubit

whose Hamiltonian is

$$\mathcal{H}_{int} = \sum_{j=1}^4 \pi \nu_j \sigma_z^j + \sum_{j < k, i=1}^4 \frac{\pi}{2} J_{jk} \sigma_z^j \sigma_z^k, \quad (6)$$

where ν_j is the chemical shift of the j th spin and J_{jk} is the spin–spin interaction (J -coupling) strength between spins j and k . To achieve a universal control on this system, a transverse magnetic field is applied at a reference frequency of ^{13}C nuclei ω_{rf} . By tuning parameters such as amplitude ω_1 , phase ϕ , and duration, the control Hamiltonian of each time step is

$$\mathcal{H}_{rf} = -\omega_1 \sum_{i=1}^4 (\cos(\omega_{rf} t + \phi) \sigma_x^i + \sin(\omega_{rf} t + \phi) \sigma_y^i). \quad (7)$$

All the experiments to prepare the quantum tetrahedra and simulate its local dynamics are divided into the following three parts:

State preparation: First, the entire system was initialized to a pseudo-pure state. With the spatial average method, the fidelity obtained is over 99% (Supplementary Note 4). Then, the system was driven into the ten invariant-tensor states from $i = A_0, A_1$ to E_0, E_1 which are shown in Fig. 2. Those transformations were implemented by ten 20 ms-shaped pulses. Those shaped pulses were all optimized by the gradient ascent pulse engineering (GRAPE) algorithm with the simulated fidelity over 99.7%²⁴. As a result, the ten experimental states obtained were denoted as ρ_i^{tetra} , where $i = A_0, A_1 \dots E_0, E_1$.

Geometry measurement: For an arbitrary density matrix represented with Pauli terms, the identity part generates no signal in the NMR system. Hence, the area operators $\hat{E}^{(k)}$ defined in Eq. (4) are unmeasurable in the experiment. Thus, in our experiment, we stress on $\cos \theta_{km}$ defined in Eq. (5), where $k \neq m$ and $k, m = 1 \dots 4$. For a qubit system, these $\cos \theta_{km}$ can be represented in terms of Pauli matrices: $\cos \theta_{km} = (\sigma_x^k \sigma_x^m + \sigma_y^k \sigma_y^m + \sigma_z^k \sigma_z^m)/6$. The observables such as $\text{Tr}[\sigma_x^k \sigma_x^m \rho_i^{\text{tetra}}] (i = A_0, A_1 \dots E_0, E_1)$ can be measured by adding assistant pulses before the measurement, which function as single-qubit rotations and were optimized by a 1 ms GRAPE pulse with a simulated fidelity over 99.7%.

We present the measured geometry properties with a three-dimensional histogram in Fig. 3, whose vertical axis represents the cosine value of angles between the face normals. In the figure, the maximum difference between experiment (colored) and theory (transparent) is within 0.08. The uncertainty came from the NMR spectrum-fitting process when using the Lorentz shape to guarantee the confidence level over 95%. With the consideration of error bars, the coincidence between experiments and theoretical simulation (Fig. 3) implies that the invariant-tensor states

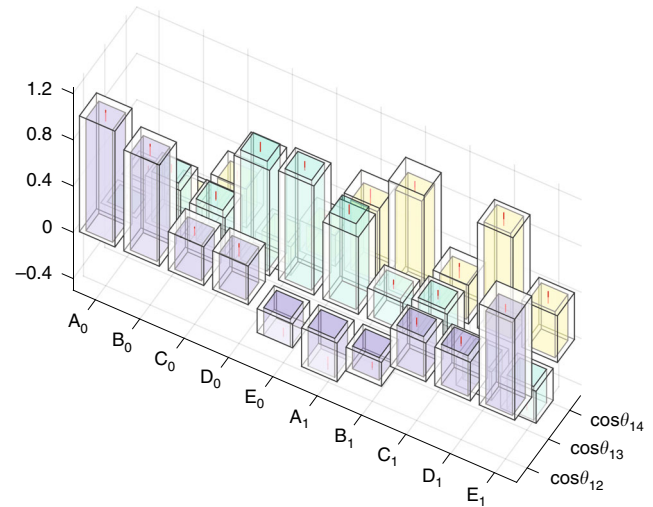


Fig. 3 Cosine values of angles between face normals in the quantum tetrahedron (cosines of dihedral angles differ by a minus sign). The results in experiments (theory) are represented by the colored (transparent) columns. Error bars came from the uncertainty when fitting nuclear magnetic resonance (NMR) spectra

prepared in our experiment match the building blocks—quantum tetrahedra.

Amplitude simulation: As the spin-network states serve as the boundary data of 3+1-dimensional quantum spacetime, the vertex amplitude defined in Eq. (3) determines the spinfoam amplitude and describes the local dynamics of QG in the 4d quantum spacetime, displaying the properties of these boundary data.

To obtain such vertex amplitudes, one needs to calculate the inner products between five different quantum tetrahedron states. This could be done in a 20-qubit quantum computer by establishing two-qubit maximally entangled state $|e_l\rangle = (|01\rangle - |10\rangle)/\sqrt{2}$ between arbitrary two tetrahedra $|i_n\rangle$, as the link l shown in Fig. 1. Nevertheless, such a quantum computer is beyond the cutting-edge technology nowadays. Alternatively, a full tomography follows our state preparation to obtain the information of quantum tetrahedron states. The fidelities between the experimentally prepared quantum tetrahedron states and the theoretical ones were also calculated. They are all above 95% (Supplementary Note 4).

By using the prepared quantum tetrahedra, we simulated the vertex amplitude in Eq. (3) by restricting $|i_n\rangle (n = 1 \dots 4)$ as the regular tetrahedra and substituted the $|i_5\rangle$ with the experimental ρ_i^{tetra} . Mixed states are inevitably introduced to the experiment

Table 1 Results of theoretical and experimentally simulated vertex amplitudes defined in Eq. (3). Vertex amplitudes are calculated from the regular tetrahedra $|i_n\rangle$ ($n = 1 \dots 4$) and experimentally prepared $|i_5\rangle$. The real and imaginary parts are listed

		A_0	B_0	C_0	D_0	E_0	A_1	B_1	C_1	D_1	E_1
Re(10^{-6})	Theory	-13.5635	-20.1590	0.0000	-26.2024	-26.5339	23.4924	18.1513	-27.1270	7.0208	-5.6401
Im(10^{-6})	Experiment	-12.74	-19.89	0.01	-24.59	-25.72	-22.16	18.73	-25.48	4.32	-3.84
	Theory	-23.4923	-18.1514	0.0000	-7.0210	5.6400	-13.5634	-20.1591	-46.9848	-26.2024	-26.5339
	Experiment	-23.67	-17.78	0.05	-7.98	6.63	13.16	-18.10	-44.14	-25.62	-25.86

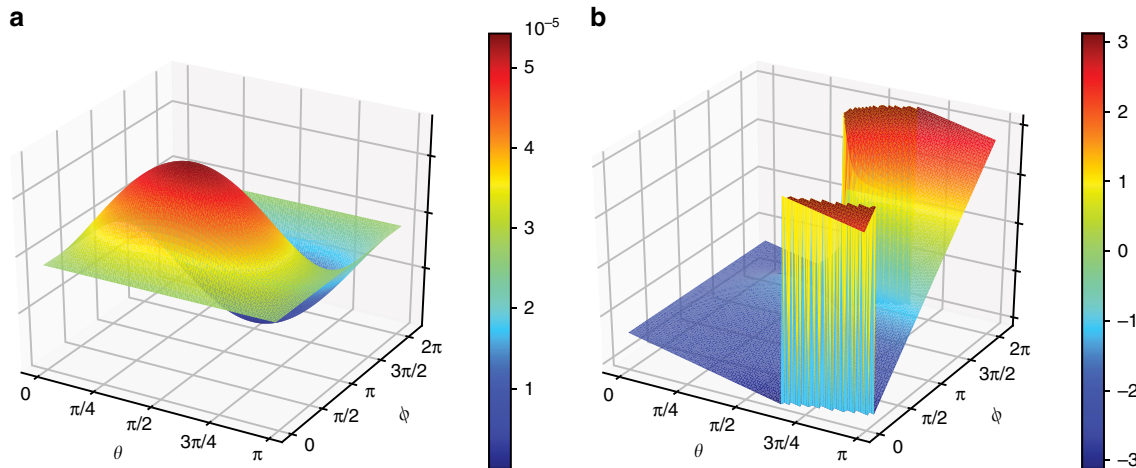


Fig. 4 Results of simulated vertex amplitudes **a** are the amplitude of Eq. (3) and **b** describe the information of its phase. θ and ϕ are the parameters of the four-qubit invariant-tensor state defined in Supplementary Note 4

because of experimental errors. To calculate the inner products in the vertex amplitude formula in Eq. (3), we purified the measured density matrices, with the method of maximal likelihood. The comparison between the experiment and the numeric simulation is listed in Table 1. The vertex amplitude $A(i_1, \dots, i_5)$ is the transition amplitude of the evolution from m to $5 - m$ quantum tetrahedra ($m < 5$) or the interaction among all five tetrahedra. As seen in Fig. 4 and Table 1, the maximum and minimum of the magnitude of the amplitude occur, respectively when ρ_i^{tetra} describes the two regular-tetrahedron states C_1 and C_0 . Table 1 also records the precise values of the amplitudes.

As a result, our experiment demonstrates that the saddle points of the amplitude indeed occur where the five interacting tetrahedra have a sensible geometric meaning, namely they glue to form a four-simplex. Such a geometrical meaning is manifest in the large- J or classical limit. To present the consequences intuitively, we also calculated the vertex amplitude based on the condition above, by varying the parameters θ and ϕ in $|i_5\rangle$. Figure 4a, b depicts the value of the simulated amplitude and phase, respectively. When $\theta = \pi/2$ and $\phi = \pi/2 (C_1)$ or $\phi = 3\pi/2 (C_0)$, the invariant-tensor states correspond to the regular tetrahedrons.

Discussion

Quantum fluctuations arise because the operators $\cos \widehat{\theta}_{km}$ do not commute, where $(k, m) = (1, 2), (1, 3), (1, 4)$. The fluctuations Δ_{km} are defined as $(\cos \widehat{\theta}_{km} - \langle i | \cos \widehat{\theta}_{km} | i \rangle)$, and we add three Δ_{km} to obtain the total quantum fluctuation (Supplementary Note 5)

$$\Delta = \frac{2}{3} + \frac{8}{3} \cos^2 \frac{\theta}{2} \sin^2 \frac{\theta}{2} (1 - \cos^2 \phi) \geq \frac{2}{3}. \quad (8)$$

The experimentally prepared states are all in the minimal fluctuation of area because the second term in Eq. (8) equals 0 (the

experimental values are listed in Supplementary Note 4). These tetrahedra are of Planck size ($\mathbf{Ar} \sim \ell_p^2$) and typically appear in quantum spacetime near the big bang or a black-hole singularity²⁵. The quantum fluctuations are quite large because the quantum tetrahedra simulated correspond to $j = 1/2$. For $j \gg 1$, we would see tetrahedron geometries with small quantum fluctuations²⁶.

By using a four-qubit quantum register in the NMR system, we created ten invariant-tensor states representing ten quantum tetrahedra with a fidelity over 95%, and subsequently measured their dihedral angles. By considering the spectrum-fitting errors, the geometrical identification implies our success in simulating quantum tetrahedra. We then simulated spin-1/2 vertex amplitudes $A(i_1, \dots, i_5)$ (in Ooguri's model). As the vertex amplitudes determine the spinfoam amplitudes and display the local dynamics, the results imply the interaction amplitude of five gluing quantum tetrahedra or display the transition from m to $(5 - m)$ quantum tetrahedra. As the first step toward exploring spin-network states and spinfoam amplitudes by using a quantum simulator, our work provides valid experimental demonstrations toward studying LQG.

Data availability

The data sets generated during and/or analyzed during the current study are available from the corresponding author upon reasonable request.

Received: 8 February 2019; Accepted: 22 August 2019;

Published online: 04 October 2019

References

1. Feynman, R. P. Simulating physics with computers. *Int. J. Theor. Phys.* **21**, 467–488 (1982).
2. Lloyd, S. Universal quantum simulators. *Science* **273**, 1073–1078 (1996).

3. Georgescu, I. M., Ashhab, S. & Nori, F. Quantum simulation. *Rev. Mod. Phys.* **86**, 153–185 (2014).
4. Vandersypen, L. M. & Chuang, I. L. Nmr techniques for quantum control and computation. *Rev. Mod. Phys.* **76**, 1037 (2005).
5. Du, J. et al. Nmr implementation of a molecular hydrogen quantum simulation with adiabatic state preparation. *Phys. Rev. Lett.* **104**, 030502 (2010).
6. Feng, G.-R., Lu, Y., Hao, L., Zhang, F.-H. & Long, G.-L. Experimental simulation of quantum tunneling in small systems. *Sci. Rep.* **3**, 2232 (2013).
7. Kiefer, C. *Quantum Gravity. International Series of Monographs on Physics.* (OUP Oxford, 2012).
8. Rovelli, C. *Quantum Gravity.* (Cambridge University Press, 2004).
9. Penrose, R. in *Angular momentum: an approach to combinatorial spacetime* (ed. Bastin, T.) *Quantum Theory and Beyond* (Cambridge University Press, 1971).
10. Han, M., Huang, W. & Ma, Y. Fundamental structure of loop quantum gravity. *Int. J. Mod. Phys.* **D16**, 1397–1474 (2007).
11. Rovelli, C. & Smolin, L. Discreteness of area and volume in quantum gravity. *Nucl. Phys. B* **442**, 593–619 (1995).
12. Barbieri, A. & Smolin, L. Quantum tetrahedra and simplicial spin networks. *Nucl. Phys.* **B518**, 714–728 (1998).
13. Rovelli, C. & Vidotto, F. *Covariant Loop Quantum Gravity: An Elementary Introduction to Quantum Gravity and Spinfoam Theory.* Cambridge Monographs on Mathematical Physics. (Cambridge University Press, 2014).
14. Perez, A. The spin foam approach to quantum gravity. *Living Rev. Rel.* **16**, 3 (2013).
15. Ooguri, H. Topological lattice models in four-dimensions. *Mod. Phys. Lett.* **A7**, 2799–2810 (1992).
16. Barrett, J. W. & Crane, L. Relativistic spin networks and quantum gravity. *J. Math. Phys.* **39**, 3296–3302 (1998).
17. Engle, J., Livine, E., Pereira, R. & Rovelli, C. LQG vertex with finite Immirzi parameter. *Nucl. Phys.* **B799**, 136–149 (2008).
18. Thiemann, T. *Modern Canonical Quantum General Relativity.* (Cambridge University Press, 2007).
19. Minkowski, H. *Ausgewählte Arbeiten zur Zahlentheorie und zur Geometrie, vol 12 of Teubner-Archiv zur Mathematik* <http://www.springerlink.com/index/10.1007/978-3-7091-9536-9>. (Springer, Vienna, 1989).
20. Freidel, L. & Livine, E. R. The fine structure of $su(2)$ intertwiners from $u(n)$ representations. *J. Math. Phys.* **51**, 082502 (2010).
21. Barrett, J. W., Fairbairn, W. J. & Hellmann, F. Quantum gravity asymptotics from the $SU(2)$ 15j symbol. *Int. J. Mod. Phys.* **A25**, 2897–2916 (2010).
22. Ashtekar, A. & Lewandowski, J. Quantum theory of geometry. 1: area operators. *Class. Quant. Grav.* **14**, A55–A82 (1997).
23. Rovelli, C. & Speziale, S. A semiclassical tetrahedron. *Class. Quant. Grav.* **23**, 5861–5870 (2006).
24. Khaneja, N., Reiss, T., Kehlet, C., Schulte-Herbrüggen, T. & Glaser, S. J. Optimal control of coupled spin dynamics: design of nmr pulse sequences by gradient ascent algorithms. *J. Magn. Reson.* **172**, 296–305 (2005).
25. Han, M. & Zhang, M. Spinfoams near a classical curvature singularity. *Phys. Rev.* **D94**, 104075 (2016).
26. Livine, E. R. & Speziale, S. A New spinfoam vertex for quantum gravity. *Phys. Rev.* **D76**, 084028 (2007).

Acknowledgements

This research was supported by CIFAR, NSERC, and Industry of Canada. K.L. and G.L. acknowledge the National Natural Science Foundation of China under grant Nos. 11175094 and 91221205 and National Key Research and Development Program of China (2017YFA0303700). Y.L. acknowledges support from the Chinese Ministry of Education under grant No. 20173080024. M.H. acknowledges support from the US National Science Foundation through grant PHY-1602867, PHY-1912278, and the start-up grant at Florida Atlantic University, USA. Y.W. thanks the hospitality of IQC and PI during his visit, where this work was partially conducted. Y.W. is also supported by the Shanghai Pujiang Program grant No. 17PJ1400700 and the NSF grant No. 11875109. D.L. is supported by the National Natural Science Foundation of China (grant Nos. 11605005, 11875159, and U1801661), Science, Technology, and Innovation Commission of Shenzhen Municipality (grant Nos. ZDSYS20170303165926217, JCYJ20170412152620376, and JCYJ20180302174036418), and Guangdong Innovative and Entrepreneurial Research Team Program (grant No. 2016ZT06D348).

Author contributions

D.L., Y.W., M.H. and R.L. conceived the experiments. K.L., D.L. and S.L. performed the experiment and analyzed the data. Y.L., J.Z. and M.H. provided theoretical support. G.L., D.R., B.Z., and R.L. supervised the project. D.L., K.L., Y.W., Y.L. and M.H. wrote the paper with feedback from all authors. The authors declare that they have no competing financial interests. Correspondence and requests for materials should be addressed to Y.W. (ydwan@fudan.edu.cn), D.L. (ludw@sustech.edu.cn), or B.Z. (zengb@uoguelph.ca). K.L., Y.L. and M.H. contributed equally to this work.

Competing interests

The authors declare no competing interests.

Additional information

Supplementary information is available for this paper at <https://doi.org/10.1038/s42005-019-0218-5>.

Correspondence and requests for materials should be addressed to Y.W., D.L. or B.Z.

Reprints and permission information is available at <http://www.nature.com/reprints>

Publisher's note Springer Nature remains neutral with regard to jurisdictional claims in published maps and institutional affiliations.



Open Access This article is licensed under a Creative Commons Attribution 4.0 International License, which permits use, sharing, adaptation, distribution and reproduction in any medium or format, as long as you give appropriate credit to the original author(s) and the source, provide a link to the Creative Commons license, and indicate if changes were made. The images or other third party material in this article are included in the article's Creative Commons license, unless indicated otherwise in a credit line to the material. If material is not included in the article's Creative Commons license and your intended use is not permitted by statutory regulation or exceeds the permitted use, you will need to obtain permission directly from the copyright holder. To view a copy of this license, visit <http://creativecommons.org/licenses/by/4.0/>.

© The Author(s) 2019